Biochemical and Biophysical Research Communications 678 (2023) 122–127

Contents lists available at ScienceDirect

Biochemical and Biophysical Research Communications

journal homepage: www.elsevier.com/locate/ybbrc

Revealing KRas4b topology on the membrane surface

Shweta Shree [a], Mark A. McLean [a], Andrew G. Stephen [b], Stephen G. Sligar [a,*]

[a] Department of Biochemistry, University of Illinois at Urbana-Champaign, Urbana, IL, 61801, United States
[b] NCI RAS Initiative, Cancer Research Technology Program, Frederick National Laboratory for Cancer Research, Leidos Biomedical Research, Inc., Frederick, MD, 21701, United States

ARTICLE INFO

Keywords:
KRas4b
Nanodisc
Cancer signaling
Membrane topology
Lipid specificity

ABSTRACT

KRas4b is a membrane-bound regulatory protein belonging to the family of small GTPases that function as a molecular switch, facilitating signal transduction from activated membrane receptors to intracellular pathways controlling cell growth and proliferation. Oncogenic mutations locking KRas4b in the active GTP state are responsible for nearly 85% of all Ras-driven cancers. Understanding the membrane-bound state of KRas4b is crucial for designing new therapeutic approaches targeting oncogenic KRas-driven signaling pathways. Extensive research demonstrates the significant involvement of the membrane bilayer in Ras-effector interactions, with anionic lipids playing a critical role in determining protein conformations The preferred topology of KRas4b for interacting with signaling partners has been a long-time question. Computational studies suggest a membrane-proximal conformation, while other biophysical methods like neutron reflectivity propose a membrane-distal conformation. To address these gaps, we employed FRET measurements to investigate the conformation of KRas4b. Using fully post-translationally modified KRas4b, we designed a Nanodisc based FRET assay to study KRas4b-membrane interactions. We suggest an extended conformation of KRas4b relative to the membrane surface. Measurement of FRET donor - acceptor distances reveal that a negatively charged membrane surface weakly favors closer association with the membrane surface. Our findings provide insights into the role of anionic lipids in determining the dynamic conformations of KRas4b and shed light on the predominant conformation of its topology on lipid headgroups.

1. Introduction

Ras mutations are drivers in nearly 30% of all human cancers [1,2]. Of the four Ras isoforms, KRas4b is the most frequently mutated isoform [3–5], and is found in about 95% of pancreatic cancer, 45% of colorectal cancer and 35% of lung cancer [6]. Ras proteins are small GTPases that function as molecular switches in signal transduction pathways and regulate cell growth, proliferation, and differentiation [7–9]. Their activity is regulated by guanine exchange factors (GEFs) which convert the inactive GDP-bound state to the active GTP-bound state, and GTPase activating proteins (GAPs) which catalyze the hydrolysis of GTP effectively converting Ras to the inactive state. The localization of Ras proteins to the plasma membrane is required for their ability to activate downstream effectors, such as RAF kinase and phosphoinositide 3-kinase (PI3K) [10–12]. Ras isoforms consist of a highly conserved "globular domain" (G-domain) and a disordered "hypervariable" region (HVR). Upon GTP binding, the two loops in the G-domain (residues 30–40 which form Switch 1 (SW1) and residues 60–70 for Switch 2 (SW2)) adopts a conformation that facilitates effector binding [13]. The HVR contains a membrane targeting motif, which in KRas4b consists of a farnesylated and carboxymethylated terminal cysteine residue and a stretch of lysine residues that form a polybasic domain (PBD) [14–16]. The insertion of the farnesyl tail and association of the lysine rich PBD with anionic lipids anchor KRas4b to the plasma membrane [17,18]. Using molecular dynamic (MD) stimulations, it has been suggested that KRas4b can adopt two predominant membrane proximal orientation states (OS1 and OS2), in which the G-domain makes direct contact with the membrane [14,19–22]. It has also been demonstrated that the HVR of KRas4b adopts distinct conformational states that mediate specific engagements with anionic lipids on the membrane, but the topology of KRas4b and orientation remain inadequately defined [18,20,22,23]. Previous modeling studies have suggested that KRas4b exists primarily on the membrane surface and is highly dynamic [18,19,23,24]. In contrast, recent findings from neutron reflectivity measurements have suggested a membrane distal conformation where the KRas4b G-domain is displaced from the membrane [25]. This extended conformation was proposed to aid recruitment of signaling proteins, via binding and

* Corresponding author. Department of Biochemistry, University of Illinois, Urbana, IL, 61801, United States.
E-mail address: s-sligar@illinois.edu (S.G. Sligar).

https://doi.org/10.1016/j.bbrc.2023.08.035
Received 4 August 2023; Accepted 16 August 2023
Available online 21 August 2023

Abbreviations

HVR	Hypervariable Region
DMPC	1,2-dimyristoyl-*sn*-glycero-3-phosphocholine
DMPS	1,2-dimyristoyl-*sn*-glycero-3-phospho-*l*-serine
GDP	Guanosine diphosphate
GTP	Guanosine triphosphate
MSP	Membrane Scaffold Protein
PIP2	phosphatidylinositol 4,5 bisphosphate
FRET	fluorescence resonance energy transfer
TAMRA	Tetramethyl rhodamine-5 C2 maleimide
SW1	Switch 1
SW2	Switch 2
OS1	Orientation state 1
OS2	Orientation state 2
GEFs	Guanine exchange factors
GAPs	GTPase activating proteins

bringing the complex to the surface. The specific role of lipid headgroups and their charge in modulating KRas4b′s association with the membrane surface also remains incompletely characterized. It is unclear whether the charge or lipid headgroups play any significant role in modulating KRas4b height above the bilayer. To help address these lacunae, we designed a fluorescence resonance energy transfer (FRET) system to help reveal the topology of KRas4b on a lipid bilayer (Nanodisc). We measured FRET by monitoring the change in lifetime of labeled KRas4b bound to labeled Nanodiscs with varying anionic lipid concentrations and different lipid headgroups. Our results demonstrate that KRas4b is primarily populated in an extended conformation, aligning with the neutron reflectivity measurements and the proposed "fly-casting model" of KRas4b on the membrane surface [25]. Our findings indicate that the negative charge on the membrane surface favors a somewhat closer approach to the membrane. As presented here, we used farnesylated and methylated KRas4b, representing the authentic version of mammalian protein, to investigate the role of anionic lipid headgroups in determining the overall topology of KRas4b on the membrane surface. By elucidating the conformational preferences of KRas4b and its interaction with the membrane surface, these measurements not only provide insights into the biology of KRas4b-membrane interactions but also sheds light on the role of lipid headgroups and the control of affinity contributing to a more comprehensive understanding of the dynamic behavior of membrane protein interactions.

2. Methods

2.1. Materials

Phospholipids 1,2-dimyristoyl-*sn*-glycero-3-phosphocholine (DMPC), 1,2-dimyristoyl-*sn*-glycero-3-phospho-*l*-serine (DMPS) and brain phosphatidylinositol 4,5 bisphosphate (PIP_2) were purchased from Avanti Polar Lipids. Tetramethyl rhodamine-5 C2 maleimide (TAMRA) was purchased from Anaspec. Alexa Fluor™ 488C^5 Maleimide was purchased from Thermofisher. Fully processed KRas4b (farnesylated and methylated) was generously provided by Frederick National Laboratory for Cancer Research (FNLCR). KRas4b-FME expression and protein production methods have been described in Ref. [26].

2.2. Purification and labeling of MSP1 D73C

Membrane scaffold proteins (MSPs) were purified as previously described [27–29]. Labeling of MSP1D1 D73C was carried out by the addition of Tris (2-carboxyethyl) phosphine hydrochloride (TCEP) to MSP1 D73C in 20 mM Tris pH 7.4, 100 mM NaCl and incubated for 15 min to reduce any disulfide bonds that may have formed. Powdered TAMRA was dissolved in dry DMSO, and a 5-fold molar excess of dye was added dropwise to the protein solution while stirring or mixing. Reactions were covered in foil and incubated at room temperature for 4 h while rotating or shaking gently, followed by overnight incubation at 4 °C. The reaction was quenched by adding 14.3 M β-mercaptoethanol (BME) stock (final concentration of 0.2 M) and rotated for another 10 min. Reactions were then incubated for 1 h at 4 °C with Amberlite XAD hydrophobic beads to remove excess dye. The protein was purified using Sephadex G25 column equilibrated in 20 mM Tris pH 7.4100 mM NaCl. Labeling efficiency and protein concentration was calculated using $\varepsilon_{280\ nm} = 21\ mM^{-1}$ for MSP, $\varepsilon_{557\ nm} = 60\ mM^{-1}$, and A280 correction factor of 0.17 for TAMRA. Final dye to protein ratios were calculated to be >90%.

2.3. Labeling of KRas4b- FME T127C118S

KRas4b- FME T127C118S protein was concentrated using a concentrator (Amicron Ultracel 10 k), and bench top centrifuge and then buffer exchanged to the labelling buffer (20 mM Hepes, 300 mM NaCl, 5 mM $MgCl_2$, 2 mM TCEP). After buffer exchange, a 5-fold molar excess of Alexa Fluor™ 488C^5 Maleimide dissolved in dry DMSO was added dropwise to the protein solution with stirring. Samples were wrapped with aluminum foil and incubated in the cold room for 2 h while gently rotating the sample. The reactions were quenched by adding BME (final concentration = 0.2 M) and rotated for another 10 min. The samples were centrifuged to remove precipitated excess dye and the supernatant was collected. The labeled protein was purified using the Superdex® 200 Increase 10/300 GL with the running buffer 20 mM HEPES, 300 mM NaCl, 5 mM $MgCl_2$. The elution profile and protein concentration were calculated by measuring absorbance of protein at 280 nm and subtracting the absorbance of the dye at 280 nm. The protein was further concentrated using Amicron ultracel 10 K concentrators as required and stored at −80 °C until further use.

2.3.1. Activity of KRas4b- FME T127C118S

A double mutant of farnesylated and methylated KRas4b was generated by introducing mutations at sites T127 and C118. The C118S mutation was introduced to remove the sole cysteine residue present on the protein surface, ensuring selective labeling at site T127 for subsequent experiments. To facilitate labeling of KRas4b at T127, the threonine residue at position 127 was mutated to cysteine. To validate the activity of the double mutant KRas4b- FME T127C118S, the release of soluble phosphate was monitored following the GTP hydrolysis using the Phosphate Senor assay (ThermoFisher). Specifically, 3 μM of KRas4b was incubated with 4.5 μM phosphate sensor protein in 50 mM HEPES, pH 7.3; 150 mM KCl, 1.5 mM $MgCl_2$, 5 mM DTT. The increase in fluorescence was measured with an excitation of 430 nm and an emission of 450 nm. The intrinsic GTPase activity of KRas4b was determined, and its rate was found to be 0.005 min^{-1}, which is consistent with the previously published data on wild-type KRas4b [26]. This observation indicates that the protein is well folded, and the introduced mutations do not induce significant conformational changes that would affect the activity of the double mutant KRas4b.

2.4. Nanodiscs preparation

The methods of Nanodisc self-assembly have been described previously in numerous literature [29–32]. Briefly, lipids dissolved in chloroform were dried under vacuum overnight and then solubilized in 200 mM sodium cholate. TAMRA labeled MSPD1 D73C is added to get 95:1 lipid to protein ratio and incubated for 15 min at room temperature. Amberlite XAD hydrophobic beads were added to remove the detergent and start the disc assembly. The mixture was incubated overnight and then purified by passing over an S200 increase size exclusion column (GE Healthcare) equilibrated in 20 mM HEPES pH 7.3150 mM NaCl.

2.5. FRET- Lifetime measurements

All Fluorescence resonance energy transfer (FRET) experiments were performed using ISS (Urbana, IL) K2 phase fluorometer equipped with a circulating water bath for temperature control using a 486 nm excitation laser and emission collected at 510 nm using a 10 nm band pass filter. Typically, 50 nM Alexa Fluor™ 488 labeled KRas4b was titrated into 10 μM TAMRA labeled Nanodisc solutions in buffer containing 20 mM HEPES pH 7.3150 mM NaCl, 1 mM $MgCl_2$ at 20 °C. To ensure complete binding of KRas4b to the Nanodiscs, a 200-fold excess of Nanodiscs was utilized. This excess favorably promoted a stoichiometry of one protein per disc, ensuring the formation of well-defined KRas4b-Nanodisc complexes. These concentrations were used to prevent multiple KRas4b molecules binding per Nanodisc surface. After mixing, samples were allowed to equilibrate, and the lifetimes were measured after 3–5 min. FRET Efficiency is calculated using the following equation:

$$E = 1 - \frac{\tau}{\tau_0} \tag{1}$$

where τ_0 is the lifetime of Alexa Fluor™ 488 labeled KRas4b bound to unlabeled Nanodiscs in the absence of an acceptor and τ is the lifetime in the presence of an acceptor i.e., TAMRA labeled Nanodiscs. The data was generated in terms of change in phase and modulation as the frequency is swept from 5 MHz to 150 MHz. Each sample was measured 10 times and the average was fitted using a standard discrete fitting model.

2.6. Förster distance determination

The Förster's radius (R_0) for TAMRA Alexa Fluor™ 488 donor acceptor pair was determined using the following equation:

$$R_0 = 0.211 \frac{\kappa^2 \varphi_D J(\lambda)}{n^4} \tag{2}$$

Here κ^2 represents a constant that relates the orientation of the transition dipoles of the donor and acceptor. We assume κ^2 to have the averaged value of 2/3 due to the local motion of the label. φ_D denotes the quantum yield of the donor Alexa Fluor® 488 which is 0.92 in solution (available at www.thermofisher.com) while n represents the refractive index of the solution, 1.34. $J(\lambda)$ is the overlap integral of the donor's emission spectrum and the acceptor's absorbance spectrum, and it can be calculated from:

$$J(\lambda) = \int_0^\infty \varepsilon_A(\lambda) \lambda^4 F_D(\lambda) d\lambda \tag{3}$$

Where $\varepsilon_A(\lambda)$ represents the absorption spectrum of the acceptor, measured in units of M^{-1} cm^{-1}, and $F_D(\lambda)$ corresponds to the emission spectrum of the donor, normalized to a unit area. The fluorescence emission spectra of Alexa Fluor® 488 were measured using 493 nm excitation and subsequently normalized to an area of 1. The absorbance spectra of TAMRA-labeled MSP1D1 D73C were measured and normalized to an extinction coefficient of 90,000 M^{-1} cm^{-1} at 572 nm. The software tool "a |e − UV–Vis-IR Spectral Software" (available at www.fluortools.com) was employed to calculate the overlap integral from the normalized spectra. By utilizing equations (2) and (3), we determined the R_0 value to be 58 Å for the TAMRA- Alexa Fluor™ 488 dye pair.

2.7. FRET-distance calculation

The efficiency of energy transfer for a single donor–acceptor pair at a fixed distance is calculated using the standard formulae:

$$E = \frac{R_0^6}{R_0^6 + r^6} \tag{4}$$

Where R_0 is Förster's radius, E is the FRET efficiency calculated using the lifetimes of donor and donor-acceptor pair and r is the distance between donor and acceptor.

2.8. Mathematical modeling of FRET distances

In order to derive the height of the FRET donor over the Nanodisc bilayer, we calculated the FRET efficiency as a function of this height H, assuming the random distribution of KRas4b on the Nanodisc surface. First, we generated 480 random points distributed along the surface of the disc. Then for each of 480 randomly selected distance coordinates on the Nanodisc surface, representing potential binding sites for KRas4b, the distance r_i (i = 1 … 480) from the FRET donor to the acceptor covalently bound to the MSP was calculated using the following equation:

$$r_i^2 = (H+1.5)^2 + D_i^2, \tag{5}$$

Where 1.5 nm is the distance along the normal to the Nanodisc surface from the bilayer surface to the position of acceptor on the MSP1 helix, and D_i is the distance from the i-th point to the acceptor in the XY plane of the Nanodisc. The diameter of one MSPD1 helix is assumed to be 1 nm and the width of Nanodisc is taken to be 4 nm. Each helix lies 1.5 nm away from corresponding nearby phosphate surface. The presence of the second acceptor on another MSP1 helix was taken into account by repeating the same procedure, except the distance to the second acceptor was calculated using the following equation:

$$r_i^2 = (H+2.5)^2 + D_i^2, \tag{6}$$

Where the position of the acceptor on the second helix adds 1 nm to the vertical projection of.

The distance vector r_i.

Using equations (5) and (6), we calculated the donor-acceptor distances for both acceptors. The FRET efficiency E_i was then calculated

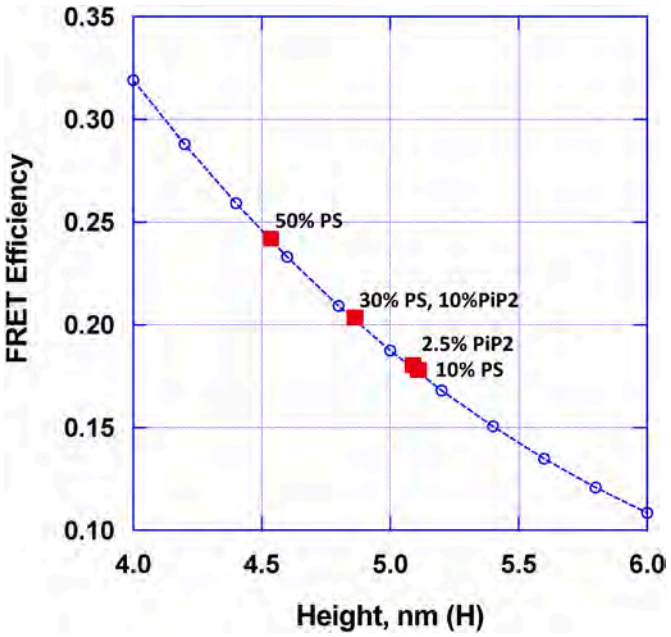

Fig. 1. Calculated dependence of average FRET efficiency between donor and acceptor (dashed curve, open circles) as a function of KRas4b height above the membrane bilayer, (see methods). The experimentally measured FRET efficiencies, indicated as red squares, obtained through FRET-lifetime measurements (Table 1). This graph then allows correlating the FRET efficiency with an average height above the membrane surface of Nanodiscs. (For interpretation of the references to color in this figure legend, the reader is referred to the Web version of this article.)

using the calculated distance r_i between donor and acceptor, and Ro = 5.8 nm, the Förster's radius:

$$E_i = Ro^6 / (Ro^6 + r_i^6) \quad (7)$$

To generate a graph that correlates the experimentally measured FRET efficiency with height above the bilayer, the averaged FRET efficiencies $<E_i>$ for all the 480 possible distance coordinates of KRas4b on the Nanodisc surface were calculated for each of two acceptors (using equation (7)) on two MSP molecules per Nanodisc to obtain the total FRET efficiency for every given H which ranges from 4 nm to 6 nm. As depicted in Fig. 1, open circles with dotted lines represent the average calculated FRET efficiency of 480 positions on the disc surface to both acceptors upon changing the height. Upon overlaying the experimentally measured FRET efficiencies (red squares) on this mathematical model, each experimentally measured FRET efficiency value corresponds to an average height of KRas4b on the bilayer. Using this method, we modeled all the potential donor acceptor distances, at different heights and different positions.

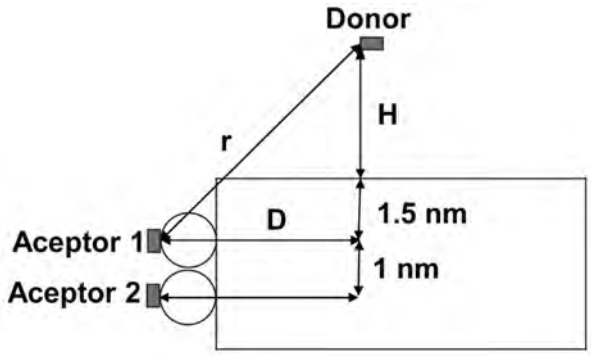

3. Results and discussion

KRas4b adopts an extended conformation and negative charge favors membrane interaction. Anionic lipids have long been known to play an important role in KRas4b interactions with negatively charged bilayers, yet the role of charged bilayers in determining the topology of KRas4b on the membrane surface has been incompletely understood. Defining the topology of KRas4b bound to the membrane is crucial to understanding its effector interactions. Previously, using a combination of fluorescence anisotropy decay experiments and molecular dynamics (MD) simulations, we predicted the role of a specific lipid head group on the affinity and orientation of KRas4b and identified residues on the protein that interact with the lipid surface [17,33]. Using frequency-domain anisotropy decay measurements, we measured the dissociation constants of KRas4b to Nanodiscs with different lipids on the membrane. We reported that the dissociation constants of fully processed KRas4b from the membrane depend significantly on the anionic lipid content [17]. The results of MD stimulations showed that the KRas4b-GDP protein displays a wide range of configurations and exhibits a relatively loose association when the membranes contain only DMPS as the anionic lipid. On the other hand, when PIP2 is present, there are long lived interactions, resulting in a more localized positioning of KRas4b as the initial contact configuration [17,33]. Therefore, the frequency of transitions between different orientations is significantly reduced with PIP2 compared to DMPS. The G-domain has direct interactions with the bilayer through multiple surfaces and in various orientations. Within microsecond timescales, two of these orientations are highly prevalent [19,22,23]. In one orientation, the canonical switch regions SW1 and SW2 are accessible for potential interactions with other proteins (OS1). However, in the alternative orientation, these switches are partially or completely occluded (OS2) [16,22,23,34]. KRas4b forms stable complexes at the membrane upon binding to different effector proteins and chaperones. For instance, PI3K is one of the major downstream effectors activated by KRas4b at the membrane surface, further phosphorylating PIP2 [35]. There are several other downstream effectors of Ras that interact at the membrane surface, most importantly the RAF kinase, which activates the MAPK pathway [36]. The bilayer plays an important role in stabilizing and activating these signaling complexes, but there is a lack of understanding of how the lipid bilayer interacts with KRas4b and dictates its topology on the surface to form stable signaling complexes with other Ras binding partners. To understand specific lipid headgroups and charge dependence, in this study we utilized Nanodiscs and their ability to precisely control lipid composition to determine the conformation dynamics of KRas4b when bound to Nanodiscs.

In this Nanodisc based FRET assay, we used Alexa Fluor™ 488 labeled KRas4b as donor and TAMRA labeled MSP as acceptor, having two acceptors per Nanodisc. Using lifetime measurements, we calculated the distance between FRET donor and acceptor at varying anionic lipid concentrations of 10%, 30%, and 50% of DMPS, with DMPC as background (Table 1). All lifetime measurements were carried out in a buffer with an ionic strength that will not alter the approach of G-domain to bilayer, because the salt effectively shields the effect of charge on protein and the negative charge of Alexa FluorTM 488 label [37]. KRas4b- FME T127C118S was labeled with Alexa FluorTM 488 and the activity of the double mutant was confirmed using a GTPase assay, providing further validation of its functionality in the experimental setup.

To understand the FRET efficiency in terms of the topology of KRas4b bound to Nanodiscs, we developed a mathematical model implemented in MATLAB (The MathWorks, Natick, MA) to calculate the average distance of the FRET donor from the acceptor. Using VMD, we modeled a fully processed KRas4b on the Nanodisc surface with the farnesyl buried in the bilayer and calculated the height of donor label (residue T127) on the G-domain to the membrane phosphates. The OS1 and OS2 PDB coordinates enabled us to estimate the vertical height for KRas4b OS1 and OS2 conformations on the membrane surface. The calculated height for a "standing up" model is 5 nm and the height for OS1 and OS2 conformations are 1.5 nm–3.5 nm respectively. Using the crystal structure of KRas4b in a fully upright conformation on the Nanodisc surface (H = 5 nm), the average FRET efficiencies for these

Table 1
Lifetime Measurement of Alexa 488 labeled KRas4b-FME using a FRET-based Nanodisc system (n = 3). The lifetime of the donor (Alexa 488 labeled KRas4b-FME) is measured when KRas4b-FME is bound to unlabeled Nanodiscs with anionic lipids and no FRET is observed. The lifetime of the donor-acceptor pair is measured when labeled KRas4b-FME is bound to TAMRA labeled Nanodiscs with anionic lipids and FRET is observed. Average FRET efficiency calculated using Donor and Donor - Acceptor pair measured lifetimes. The distance is calculated using equation (4) with $R_0 = 5.8$ nm. Average G-domain height above the bilayer surface is calculated from our mathematical model using experimentally determined FRET efficiencies.

Anionic Lipid Concentration	Donor Lifetime (ns)	Donor + Acceptor Lifetime (ns)	Avg. FRET Efficiency	Average G- Domain Height Above Bilayer (nm) See Fig. 1
10% DMPS	**3.8 ± 0.01**	**3.13 ± 0.01**	**0.178 ± 0.001**	**5.10**
30% DMPS	**3.8 ± 0.01**	**3.03 ± 0.01**	**0.202 ± 0.002**	**4.87**
50% DMPS	**3.8 ± 0.01**	**2.91 ± 0.01**	**0.241 ± 0.001**	**4.55**
2.5% PIP2	**3.9 ± 0.01**	**3.19 ± 0.01**	**0.18 ± 0.005**	**5.09**
10% PIP2	**3.9 ± 0.01**	**3.11 ± 0.01**	**0.203 ± 0.003**	**4.86**

models were calculated to be 0.119 and 0.068 for the two acceptors on the Nanodisc belt. By summing the modeled FRET efficiencies, we determined the distance between donor on KRas4b and acceptor on Nanodisc (see methods). The averaged total FRET efficiencies for all the 480 possible distance coordinates of KRas4b on the Nanodisc surface was plotted as a function of height above the bilayer (Fig. 1).

We overlayed the experimentally measured FRET efficiencies to this model and calculated the height of KRas4b over the Nanodisc. According to this model, the height of KRas4b over the Nanodisc bilayer ranged from 5.10 nm to 4.55 nm as anionic lipid concentration increases, which clearly indicates a charge dependence of KRas4b topology on the Nanodisc surface (Table 1). These measured average heights correspond to an extended conformation of KRas4b on the nanodisc surface and not to the membrane proximal conformations (OS1 and OS2), as depicted in Fig. 2. Therefore, we propose that the extended conformation of KRas4b is the predominant topology compared to other membrane proximal positions. To understand specific lipid headgroup dependence, we used PIP2 lipids in Nanodiscs which is known to be important for Son of Sevenless recruitment to the plasma membrane and also a substrate for PI3K, which is a downstream effector for activated KRas4b [38]. To investigate further the role of PIP2 in determining the topology of KRas4b on the membrane surface, we used the FRET-based assay to measure the distance between donor and acceptor and extract the height of the G-domain from the membrane surface. The measured distances for 2.5% PIP2 and 10% PIP2 with DMPC background on Nanodiscs correlate to the distances measured with the similar charged DMPS Nanodiscs. As shown in Table 1, the measured height of KRas4b from the membrane surface indicates a small, but significant, anionic lipid concentration dependence that is similar for PIP2 and PS headgroups. The two orientation states previously discussed, OS1 and OS2, have rapid transitions on the membrane surface and were predicted to occur at a sub - microsecond timescale [18,19,22,23]. Since it is evident that these conformations are dynamic on the surface, it justifies the averaging method we used in this study to understand the topology of KRas4b on Nanodiscs. At the timescale of these measurements, the average FRET efficiencies includes the ensemble of the dynamic interconversion of KRas4b on the Nanodisc surface. Our results suggest that KRas4b is predominantly populated in a membrane-distal state when anionic lipids are present, with multiple orientations to facilitate effector binding. Additionally, the measured FRET efficiencies show that negatively charged membrane surface favors membrane proximal conformations and reorients the ensemble average configuration closer to membrane, suggesting membrane interactions. Interestingly, the subtle change in FRET represents a re-distribution of these configurations in the presence of anionic lipids and does not depend significantly on the specific lipid headgroups. The slope depicted in Fig. 2 cannot definitively determine whether the observed changes in FRET efficiency are primarily driven by the HVR's proximity to the bilayer or the orientation changes involving the G-domain. These ensemble configurations imply that the lipid headgroup composition may not be the sole determinant of KRas4b topology. Our study, employing a FRET-based Nanodisc assay, observed differences in FRET efficiency between Nanodiscs with similar charges but distinct lipid headgroups which highlights the complexity of protein-membrane interactions and suggest the involvement of other factors. Specifically, the results of our FRET assay involving 10% PIP2 Nanodiscs, which have similar charge properties to 30% DMPS Nanodiscs, suggest that charge and not lipid head group identity is the major influence on the average distance of KRas4b from the membrane. Anionic lipids on the membrane surface increases the affinity of KRas4b to the membrane surface [17]. Therefore, the distribution of the distal vs proximal population is dependent on the anionic lipids. Overall, these results demonstrate that anionic lipids influence the proximal or distal population of KRas4b.

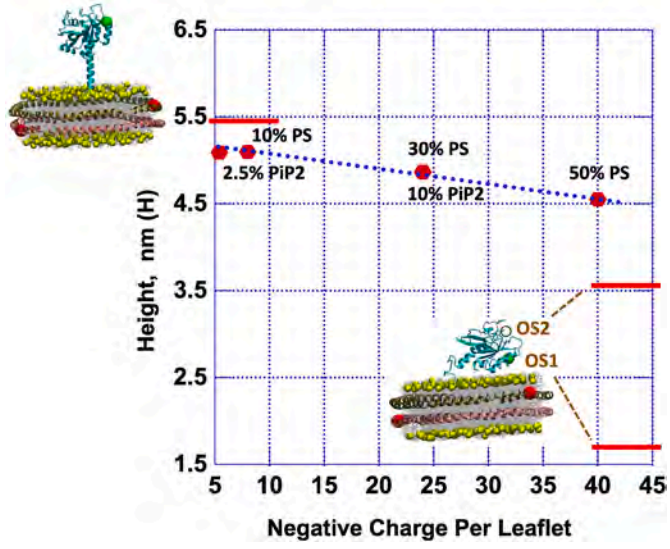

Fig. 2. Dependence of KRas4b height above the membrane bilayer as a function of the formal charge on the Nanodisc. Indicated are the calculated heights for the extended and membrane local conformations as determined from molecular dynamics simulations (see text).

In summary, our study utilized a novel FRET-based Nanodisc-based assay to analyze protein-membrane interactions. In conclusion, our results reveal the most prevalent conformation of KRas4b, which manifests the extended configuration bound to Nanodisc with precisely controlled lipid composition. These findings contribute to a better understanding of the structural dynamics and interactions of KRas4b when bound to Nanodiscs, which has implications for studying its functional roles in various biological processes.

Declaration of competing interest

All authors declare no conflict of interest.

Acknowledgements

We thank Dr. Ilia Denisov and Dr. Yelena Grinkova from the University of Illinois at Urbana-Champaign for helping with MATLAB modeling, numerous insightful discussions, and helpful suggestions. We express gratitude to the Gorfe Group for their generous provision of the OS1 and OS2 PDB coordinates and Dr. Rebika Shrestha for her advise on labeling KRas-FME. We gratefully acknowledge the support of a MIRA grant from the National Institutes of Health (R35 GM118145) for funding this research. This project has been funded in whole or in part with Federal funds from the National Cancer Institute, National Institutes of Health, under Contract No. 75N91019D00024. The content of this publication does not necessarily reflect the views or policies of the Department of Health and Human Services, nor does mention of trade names, commercial products or organizations imply endorsement by the U.S. Government. We extend special thanks to the NCI RAS Initiative at the Frederick National Laboratory for Cancer Research, led by Dr. Frank McCormick and Dr. Dwight Nissley, and their team members for their valuable collaboration. We also thank Vanessa Wall, Kelly Snead, Shelley Perkins, William K Gillette and Dominic Esposito for production of the KRas4b protein used in this work. Finally, we thank Dana Rabara for performing the Phosphate senor assays on the KRas4b proteins.

References

[1] D. Uprety, A.A. Adjei, KRAS: from undruggable to a druggable Cancer Target, Cancer Treat Rev. 89 (2020), 102070, https://doi.org/10.1016/j.ctrv.2020.102070.

[2] S.A. Forbes, N. Bindal, S. Bamford, C. Cole, C.Y. Kok, D. Beare, M. Jia, R. Shepherd, K. Leung, A. Menzies, J.W. Teague, P.J. Campbell, M.R. Stratton, P.A. Futreal, COSMIC: mining complete cancer genomes in the catalogue of somatic mutations in cancer, Nucleic Acids Res. 39 (2011) 945–950, https://doi.org/10.1093/nar/gkq929.

[3] L. Huang, Z. Guo, F. Wang, L. Fu, KRAS mutation: from undruggable to druggable in cancer, Signal Transduct. Targeted Ther. 6 (2021) 386, https://doi.org/10.1038/s41392-021-00780-4.
[4] M. Zuberi, I. Khan, J.P. O'Bryan, Inhibition of RAS: proven and potential vulnerabilities, Biochem. Soc. Trans. 48 (2020) 1831–1841, https://doi.org/10.1042/BST20190023.
[5] V. Aran, K-Ras4A, Lead or supporting role in cancer biology? Front. Mol. Biosci. 8 (2021), 729830 https://doi.org/10.3389/fmolb.2021.729830.
[6] H.-Z. Wu, J.-Q. Xiao, S.-S. Xiao, Y. Cheng, KRAS: a promising therapeutic target for cancer treatment, Curr. Top. Med. Chem. 19 (2019) 2081–2097, https://doi.org/10.2174/1568026619666190905164144.
[7] D.K. Simanshu, D.V. Nissley, F. McCormick, RAS proteins and their regulators in human disease, Cell 170 (2017) 17–33, https://doi.org/10.1016/j.cell.2017.06.009.
[8] W.E. Kattan, J.F. Hancock, RAS Function in cancer cells: translating membrane biology and biochemistry into new therapeutics, Biochem. J. 477 (2020) 2893–2919, https://doi.org/10.1042/BCJ20190839.
[9] F. McCormick, A brief history of RAS and the RAS Initiative, in: Adv Cancer Res, Academic Press Inc., 2022, pp. 1–27, https://doi.org/10.1016/bs.acr.2021.07.003.
[10] H. Lavoie, M. Therrien, Regulation of RAF protein kinases in ERK signaling, Nat. Rev. Mol. Cell Biol. 16 (2015) 281–298, https://doi.org/10.1038/nrm3979.
[11] D. Stokoe, S.G. Macdonald, K. Cadwallader, M. Symons, J.F. Hancock, Activation of raf as a result of recruitment to the plasma membrane, Science 264 (1994) 1463–1467, https://doi.org/10.1126/science.7811320.
[12] M.T. Mazhab-Jafari, C.B. Marshall, M.J. Smith, G.M.C. Gasmi-Seabrook, P. B. Stathopulos, F. Inagaki, L.E. Kay, B.G. Neel, M. Ikura, Oncogenic and RASopathy-associated K-RAS mutations relieve membrane-dependent occlusion of the effector-binding site, Proc. Natl. Acad. Sci. U.S.A. 112 (2015) 6625–6630, https://doi.org/10.1073/pnas.1419895112.
[13] M.E. Welsch, A. Kaplan, J.M. Chambers, M.E. Stokes, P.H. Bos, A. Zask, Y. Zhang, M. Sanchez-Martin, M.A. Badgley, C.S. Huang, T.H. Tran, H. Akkiraju, L.M. Brown, R. Nandakumar, S. Cremers, W.S. Yang, L. Tong, K.P. Olive, A. Ferrando, B. R. Stockwell, Multivalent small-molecule pan-RAS inhibitors, Cell 168 (2017) 878–889, https://doi.org/10.1016/j.cell.2017.02.006.
[14] Y. Zhou, P. Prakash, A.A. Gorfe, J.F. Hancock, Ras and the plasma membrane: a complicated relationship, Cold Spring Harb. Perspect Med. 8 (2018) a031831, https://doi.org/10.1101/cshperspect.a031831.
[15] M. Haidar, P. Jacquemin, Past and future strategies to inhibit membrane localization of the kras oncogene, Int. J. Mol. Sci. 22 (2021), 13193, https://doi.org/10.3390/ijms222413193.
[16] S. Cao, S. Chung, S.J. Kim, Z. Li, D. Manor, M. Buck, K-Ras G-domain binding with signaling lipid phosphatidylinositol (4, 5)-phosphate (PIP2): membrane association, protein orientation, and function, J. Biol. Chem. 294 (2019) 7068–7084, https://doi.org/10.1074/jbc.RA118.004021.
[17] M.C. Gregory, M.A. McLean, S.G. Sligar, Interaction of KRas4b with anionic membranes: a special role for PIP2, Biochem. Biophys. Res. Commun. 487 (2017) 351–355, https://doi.org/10.1016/j.bbrc.2017.04.063.
[18] K.-Y. Lee, M. Ikura, C.B. Marshall, The Self-Association of the KRAS4b Protein Is Altered by Lipid-Bilayer Composition and Electrostatics, Angewandte Chemie International Edition, 2023, e202218698, https://doi.org/10.1002/anie.202218698.
[19] P. Prakash, A.A. Gorfe, Probing the conformational and energy landscapes of KRAS membrane orientation, J. Phys. Chem. B 123 (2019) 8644–8652, https://doi.org/10.1021/acs.jpcb.9b05796.
[20] M.K. Araya, A.A. Gorfe, Phosphatidylserine and phosphatidylethanolamine asymmetry have a negligible effect on the global structure, dynamics, and interactions of the KRAS lipid anchor, J. Phys. Chem. B 126 (2022) 4491–4500, https://doi.org/10.1021/acs.jpcb.2c01253.
[21] Y. Zhou, A.A. Gorfe, J.F. Hancock, RAS nanoclusters selectively sort distinct lipid headgroups and acyl chains, Front. Mol. Biosci. 8 (2021), 686338, https://doi.org/10.3389/fmolb.2021.686338.
[22] P. Prakash, Y. Zhou, H. Liang, J.F. Hancock, A.A. Gorfe, Oncogenic K-Ras binds to an anionic membrane in two distinct orientations: a molecular dynamics analysis, Biophys. J. 110 (2016) 1125–1138, https://doi.org/10.1016/j.bpj.2016.01.019.
[23] C. Neale, A.E. García, Methionine 170 is an environmentally sensitive membrane anchor in the disordered HVR of K-Ras4B, J. Phys. Chem. B 122 (2018) 10086–10096, https://doi.org/10.1021/acs.jpcb.8b07919.
[24] V.A. Ngo, A.E. Garcia, Millisecond molecular dynamics simulations of KRas-dimer formation and interfaces, Biophys. J. 121 (2022) 3730–3744, https://doi.org/10.1016/j.bpj.2022.04.026.
[25] Q.N. Van, C.A. López, M. Tonelli, A.G. Stephen, Uncovering a membrane-distal conformation of KRAS available to recruit RAF to the plasma membrane, Proc. Natl. Acad. Sci. USA 117 (2020) 24258–24268, https://doi.org/10.1073/pnas.2006504117/-/DCSupplemental.
[26] W.K. Gillette, D. Esposito, M. Abreu Blanco, P. Alexander, L. Bindu, C. Bittner, O. Chertov, P.H. Frank, C. Grose, J.E. Jones, Z. Meng, S. Perkins, Q. Van, R. Ghirlando, M. Fivash, D.V. Nissley, F. McCormick, M. Holderfield, A.G. Stephen, Farnesylated and methylated KRAS4b: high yield production of protein suitable for biophysical studies of prenylated protein-lipid interactions, Sci. Rep. 5 (2015), 15916, https://doi.org/10.1038/srep15916.
[27] I.G. Denisov, Y.V. Grinkova, A.A. Lazarides, S.G. Sligar, Directed self-assembly of monodisperse phospholipid bilayer nanodiscs with controlled size, J. Am. Chem. Soc. 126 (2004) 3477–3487, https://doi.org/10.1021/ja0393574.
[28] T.H. Bayburt, Y.V. Grinkova, S.G. Sligar, Self-assembly of discoidal phospholipid bilayer nanoparticles with membrane scaffold proteins, Nano Lett. 2 (2002) 853–856, https://doi.org/10.1021/nl025623k.
[29] T.K. Ritchie, Y.V. Grinkova, T.H. Bayburt, I.G. Denisov, J.K. Zolnerciks, W. M. Atkins, S.G. Sligar, Chapter 11 reconstitution of membrane proteins in phospholipid bilayer nanodiscs, Methods Enzymol. 464 (2009) 211–231, https://doi.org/10.1016/S0076-6879(09)64011-8.
[30] T.H. Bayburt, S.G. Sligar, Membrane protein assembly into Nanodiscs, FEBS Lett. 584 (2010) 1721–1727, https://doi.org/10.1016/j.febslet.2009.10.024.
[31] I.G. Denisov, S.G. Sligar, Nanodiscs for structural and functional studies of membrane proteins, Nat. Struct. Mol. Biol. 23 (2016) 481–486, https://doi.org/10.1038/nsmb.3195.
[32] M.A. Schuler, I.G. Denisov, S.G. Sligar, Nanodiscs as a new tool to examine lipid-protein interactions, Methods Mol. Biol. 974 (2013) 415–433, https://doi.org/10.1007/978-1-62703-275-9_18.
[33] M.A. McLean, A.G. Stephen, S.G. Sligar, PIP2 influences the conformational dynamics of membrane-bound KRAS4b, Biochemistry 58 (2019) 3537–3545, https://doi.org/10.1021/acs.biochem.9b00395.
[34] X. Gu, D. Liu, Y. Yu, H. Wang, D. Long, Quantitative paramagnetic NMR-based analysis of protein orientational dynamics on membranes: dissecting the KRas4B-membrane interactions, J. Am. Chem. Soc. 145 (2023) 10295–10303, https://doi.org/10.1021/jacs.3c01597.
[35] R. Nussinov, G. Wang, C.J. Tsai, H. Jang, S. Lu, A. Banerjee, J. Zhang, V. Gaponenko, Calmodulin and PI3K signaling in KRAS cancers, Trends Cancer 3 (2017) 214–224, https://doi.org/10.1016/j.trecan.2017.01.007.
[36] L. Li, S. Möbitz, R. Winter, Characterization of the spatial organization of raf isoforms interacting with K-Ras4B in the lipid membrane, Langmuir 36 (2020) 5944–5953, https://doi.org/10.1021/acs.langmuir.0c00770.
[37] A.M. Smith, A.A. Lee, S. Perkin, The electrostatic screening length in concentrated electrolytes increases with concentration, J. Phys. Chem. Lett. 7 (2016) 2157–2163, https://doi.org/10.1021/acs.jpclett.6b00867.
[38] J. Gureasko, W.J. Galush, S. Boykevisch, H. Sondermann, D. Bar-Sagi, J.T. Groves, J. Kuriyan, Membrane-dependent signal integration by the Ras activator Son of sevenless, Nat. Struct. Mol. Biol. 15 (2008) 452–461, https://doi.org/10.1038/nsmb.1418.